Reverse genetics with a full-length infectious cDNA of the Middle East respiratory syndrome coronavirus

Trevor Scobey[a], Boyd L. Yount[a], Amy C. Sims[a], Eric F. Donaldson[a], Sudhakar S. Agnihothram[a], Vineet D. Menachery[a], Rachel L. Graham[a], Jesica Swanstrom[a], Peter F. Bove[b], Jeeho D. Kim[c], Sonia Grego[d], Scott H. Randell[c], and Ralph S. Baric[a,e,1]

Departments of [a]Epidemiology, [c]Cell Biology and Physiology, and [e]Microbiology and Immunology and [b]Cystic Fibrosis/Pulmonary Research and Treatment Center, University of North Carolina at Chapel Hill, Chapel Hill, NC 27599-7435; and [d]Center for Materials and Electronic Technologies, Research Triangle International, Durham, NC 27709

Edited by Peter Palese, Mount Sinai School of Medicine, New York, NY, and approved August 13, 2013 (received for review June 18, 2013)

Severe acute respiratory syndrome with high mortality rates (~50%) is associated with a novel group 2c betacoronavirus designated Middle East respiratory syndrome coronavirus (MERS-CoV). We synthesized a panel of contiguous cDNAs that spanned the entire genome. Following contig assembly into genome-length cDNA, transfected full-length transcripts recovered several recombinant viruses (rMERS-CoV) that contained the expected marker mutations inserted into the component clones. Because the wild-type MERS-CoV contains a tissue culture-adapted T1015N mutation in the S glycoprotein, rMERS-CoV replicated ~0.5 log less efficiently than wild-type virus. In addition, we ablated expression of the accessory protein ORF5 (rMERS●ORF5) and replaced it with tomato red fluorescent protein (rMERS-RFP) or deleted the entire ORF3, 4, and 5 accessory cluster (rMERS-ΔORF3–5). Recombinant rMERS-CoV, rMERS-CoV●ORF5, and MERS-CoV-RFP replicated to high titers, whereas MERS-ΔORF3–5 showed 1–1.5 logs reduced titer compared with rMERS-CoV. Northern blot analyses confirmed the associated molecular changes in the recombinant viruses, and sequence analysis demonstrated that RFP was expressed from the appropriate consensus sequence AACGAA. We further show dipeptidyl peptidase 4 expression, MERS-CoV replication, and RNA and protein synthesis in human airway epithelial cell cultures, primary lung fibroblasts, primary lung microvascular endothelial cells, and primary alveolar type II pneumocytes, demonstrating a much broader tissue tropism than severe acute respiratory syndrome coronavirus. The availability of a MERS-CoV molecular clone, as well as recombinant viruses expressing indicator proteins, will allow for high-throughput testing of therapeutic compounds and provide a genetic platform for studying gene function and the rational design of live virus vaccines.

emerging pathogen | zoonosis | synthetic genome

Emerging respiratory virus infections can cause considerable morbidity and mortality in human populations. Some, including influenza A viruses and human coronaviruses (CoVs), can spread rapidly and cause acute lung injury and its more severe form, acute respiratory distress syndrome (ARDS). These devastating end-stage lung diseases are often associated with high mortality rates (~30–50%) and can progress to chronic conditions such as pulmonary fibrosis (1). CoVs frequently transmit between species (2–4). Divided into three main groups, the betacoronaviruses represent a large collection of phylogenetically distant strains that include several human coronaviruses (HCoVs) such as HCoV OC43, HCoV HKU1 (group 2a), and the severe acute respiratory syndrome coronavirus (SARS-CoV) (group 2b) (5). In 2003, SARS-CoV emerged from zoonotic sources in China and caused atypical pneumonia and ARDS with 10% mortality rates (5). In 2012, a new group 2c betacoronavirus was detected in the Middle East (3). Designated MERS-CoV (Middle East respiratory syndrome coronavirus), it has caused at least 114 confirmed cases with 54 deaths as of September 10, 2013. The virus replicates efficiently in human airway epithelial cells (HAEs) and uses human and bat dipeptidyl peptidase 4 (DPP4) as receptors for entry (6, 7). Human-to-human transmission, coupled with the unusual severity and high mortality rates, dictates a need for key resources for the testing of MERS-CoV therapeutics and vaccines (8).

The 30,119-nt MERS-CoV genome encodes a typical portfolio of ORFs expressed from both genome-length (ORF1a/1b) (9) and subgenomic-length mRNAs (sgRNAs), which are arranged in a nested set from the 3′ end of the genome. The MERS-CoV transcription regulatory sequence (TRS) is predicted to be AACGAA, but remains poorly defined in culture. In addition to the classic structural proteins—a 180/90-kDa spike glycoprotein (S), an ~23-kDa membrane glycoprotein (M), a small envelope protein (E), and an ~50-kDa nucleocapsid protein (N)—MERS-CoV also encodes at least four group-specific ORFs designated ORF3, ORF4a, ORF4b, and ORF5. Previously, we constructed or synthesized full-length infectious clones from several CoVs, including SARS-CoV, HCoV NL63, and HKU3 (BAT-SRBD) (10–12). In this manuscript, we describe the synthesis and assembly of a full-length molecular clone for MERS-CoV and show that wild-type MERS-CoV (EMC2012 substrain) has evolved a unique tissue culture-adapted mutation in the S glycoprotein that is not present in the recombinant virus derived from the molecular clone. Recombinant viruses were also isolated that express a red fluorescent indicator, tomato red (red fluorescent protein; RFP), from sgRNA. In addition, we also generate mutants lacking one or more of the MERS-CoV group-specific ORFs. The availability

Significance

The identification of a novel, emerging human coronavirus with ~50% mortality, designated Middle East respiratory syndrome coronavirus (MERS-CoV), emphasizes the importance of the rapid development of reagents that can be used to (*i*) characterize the replication and pathogenesis of emerging pathogens and (*ii*) develop therapeutics for treatment. In this report, we describe the development of a cassette-based infectious cDNA clone of MERS-CoV and verify that it functions similarly to the wild-type isolate in terms of replication, protein and RNA expression, and spike attachment protein processing. We also show that the virus replicates preferentially in differentiated primary lung cells.

Author contributions: T.S., B.L.Y., and R.S.B. designed research; T.S., B.L.Y., A.C.S., E.F.D., S.S.A., V.D.M., R.L.G., J.S., and J.D.K. performed research; P.F.B., S.G., and S.H.R. contributed new reagents/analytic tools; T.S., B.L.Y., A.C.S., E.F.D., S.S.A., V.D.M., R.L.G., J.S., and R.S.B. analyzed data; and T.S., A.C.S., E.F.D., R.L.G., J.D.K., and R.S.B. wrote the paper.

The authors declare no conflict of interest.

This article is a PNAS Direct Submission.

Freely available online through the PNAS open access option.

[1]To whom correspondence should be addressed. E-mail: rbaric@ad.unc.edu.

This article contains supporting information online at www.pnas.org/lookup/suppl/doi:10.1073/pnas.1311542110/-/DCSupplemental.

MICROBIOLOGY

of a molecular clone for MERS-CoV, along with marker and deletion viruses, provides opportunities for understanding novel gene functions, tools for high-throughput screening of antiviral drugs, and essential reagents for the rational design of candidate live-attenuated virus vaccines.

Results

Design of MERS-CoV Full-Length cDNAs. Rapid response and control of emerging respiratory viruses require high-throughput strategies for the manipulation and recovery of recombinant viruses by reverse genetic strategies. The MERS-CoV genome was initially synthesized as a panel of six contiguous cDNAs (A–F) that span the genome and are linked by class II restriction endonuclease sites (BglI-GCCNNNN$^{\downarrow}$NGGC), which cleave at symmetrical palindromic sequences but leave different asymmetric 3-nt overhangs. Due to instability in the plasmid, the D fragment was split into two separate fragments, resulting in seven total cDNA cassettes (Fig. 1). Thus, rational cDNA design allows for the systematic, directional, and efficient assembly of the individual MERS A–F cDNAs into a genome-length cDNA by in vitro ligation (12). In addition, naturally occurring BglI sites were removed by G-C and C-T changes at positions 494 and 17713, respectively, and an A-G change was introduced at position 2393 to ablate a potential T7 pause site in the derived synthetic molecular clone (12). The MERS D fragment was unstable in microbial vectors and was thus bisected into two pieces, designated MERS D1 and MERS D2, which were very stable. BglI sites were engineered by introducing silent mutations between the A/B, B/C, C/D1, D1/D2, D2/E, and E/F junctions (Fig. 1). The MERS A fragment contains a T7 start site, whereas the F subclone terminates in 25 T residues, allowing for in vitro transcription of capped, polyadenylated transcripts.

Characterization of Recombinant Viruses. To assemble the MERS-CoV molecular clone, each subclone was digested with BglI, purified, and ligated, and the resulting product was used as a template for in vitro transcription. Because N gene transcripts enhance the infectivity of CoV full-length transcripts (12), recombinant (rMERS-CoV) transcripts were mixed with capped N transcripts and electroporated into Vero cells. Within 48–72 h posttransfection, cytopathic effects and leader-containing transcripts were detected within transfected cultures but not in controls.

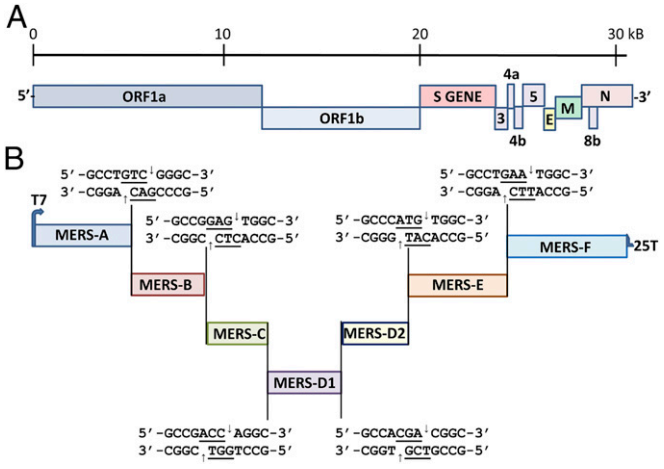

Fig. 1. Organization of the MERS-CoV molecular clone. (*A*) The organization of the MERS-CoV genome. (*B*) The full-length MERS-CoV genome was ultimately divided into seven contiguous cDNAs designated MERS A–F and flanked by unique BglI sites that allow for directed assembly of a full-length cDNA: MERS A (nucleotides 1–4692), MERS-B (4693–8811), MERS-C (8812–12258), MERS-D1 (12259–15470), MERS-D2 (15471–18806), MERS-E (18807–24397), and MERS-F (24398–30119).

rMERS-CoV replicated to titers that approach 10^7 to 10^8 plaque-forming units/mL (pfu/mL) and formed small plaques in Vero 81 cells (Figs. 2 and 3). rMERS-CoV, but not wild-type virus, should encode several unique marker mutations at the junctions associated with the assembly of the component clones. Therefore, RT-PCR was used to generate cDNA amplicons, which were purified and then subjected to restriction fragment length polymorphism (RFLP) analysis with BglI. MERS-CoV contains a BglI site at position 17717 that was ablated in rMERS-CoV (Fig. 2*B*). In contrast, rMERS-CoV contains a BglI site inserted between the component E/F junctions (Fig. 2*C*), a genotype that was subsequently verified by genome-length sequence analysis.

Interestingly, wild-type MERS-CoV appeared to replicate ~0.5 log more efficiently and formed larger plaques than rMERS-CoV (Figs. 2 and 3). Genome-length sequence analysis of our passage 9 wild-type MERS-CoV stock revealed a unique consensus T1015N change in the S glycoprotein that was not present in the published sequence. To evaluate whether this consensus mutation altered virus growth kinetics or plaque morphology in vitro, we introduced this mutation into the molecular clone and isolated a recombinant virus (rMERS-CoV T1015N). rMERS-CoV T1015N more closely replicated wild-type virus replication kinetics and plaque formation (Figs. 2*D* and 3*E*). These data suggest that T1015N is a tissue culture-adapted mutation that arose during serial in vitro passage.

rMERS-CoV Derivative Virus Phenotypes. The MERS-CoV genome encodes several accessory ORFs of unknown function. To evaluate the roles of these accessory ORFs in MERS-CoV replication, we introduced a stop codon into ORF5 at nucleotide $A_{27162}G$ (rMERS-CoV•ORF5), which truncated ORF5, replaced ORF5 with the RFP gene (rMERS-CoV-RFP), or deleted the downstream subgenomic ORFs 3, 4a, 4b, and 5 (rMERS-CoV-ΔORF3–5). Following electroporation of full-length transcripts into Vero cells, recombinant viruses were isolated. Compared with rMERS-CoV, rMERS-CoV•ORF5 and rMERS-CoV-RFP replicated to titers from 10^7 to 10^8 pfu/mL. In contrast, the replication of rMERS-CoV-ΔORF3–5 was significantly reduced by ~1–1.5 logs in Vero cells (Fig. 2*A*). Consonant with the presence of sgRNA transcripts encoding RFP, fluorescent microscopy revealed RFP fluorescence at different times postinfection in rMERS-CoV-RFP but not in rMERS-CoV– or wild-type control-infected cultures (Fig. 3 *A–D*). To evaluate virus RNA synthesis, Northern blot analyses revealed the expected set of appropriately sized RNAs in wild-type MERS-CoV–, rMERS-CoV–, rMERS-CoV-RFP–, and rMERS-CoV•ORF5–infected cells, which included genome-length RNA and seven sgRNAs (Fig. 4*A*). As RFP and ORF5 are of similar size, we did not note any visible alterations in the size of sgRNA5 between these two viruses. In contrast, rMERS-CoV-ΔORF3–5 removed several ORFs and TRSs from the genome, resulting in a loss of sgRNAs 3, 4, and 5 and increased expression and mobility of sgRNA2 (S glycoprotein) (Fig. 4*A*).

To evaluate recombinant virus structural protein expression, we cloned and expressed the MERS-CoV S and N proteins in Venezuelan equine encephalitis virus strain 3526 replicon constructs [virus replicon particle (VRP)-S, VRP-N], inoculated mice, and isolated antisera against these viral proteins. Using Western blot analysis, we confirmed robust S-glycoprotein and N-protein expression in wild-type MERS-CoV–, rMERS-CoV–, rMERS-CoV•ORF5–, rMERS-CoV-RFP–, and rMERS-CoV-ΔORF3–5–infected cells (Fig. 4*B*). Interestingly, increased S-glycoprotein expression was noted in rMERS-CoV-Δ3–5–infected cells, a phenotype coincident with increased sgRNA2 expression (Fig. 4*B*). The MERS-CoV S glycoproteins are cleaved more efficiently at later times and were heavily glycosylated, as evidenced by increased electrophoretic mobility following peptide-N-glycosidase F (PNGase F) treatment (Fig. S1). As downstream

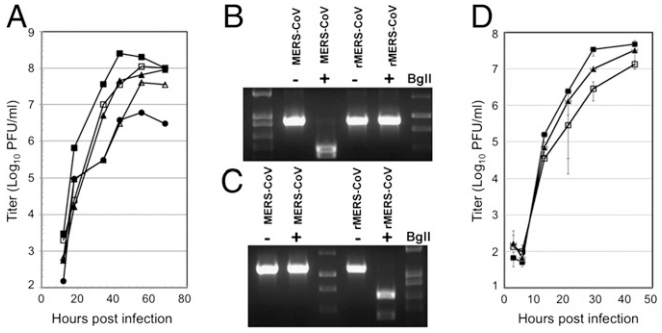

Fig. 2. Recombinant virus growth. (*A*) Cultures of Vero 81 cells were infected with MERS-CoV, rMERS-CoV, rMERS-CoV•ORF5, rMERS-CoV-RFP, and rMERS-CoV-ΔORF3–5 at an MOI of 0.01. Virus samples were harvested at different times postinfection and titered by plaque assay (■, MERS-CoV; □, rMERS-CoV; ▲, rMERS-CoV•ORF5; Δ, rMERS-CoV-RFP; ●, rMERS-CoV-ΔORF3–5). (*B*) RFLP analysis spanning a naturally occurring BglI site at ~17,717 bp that is ablated in rMERS-CoV; uncut vs. digested with BglI. (*C*) RFLP analysis across the engineered rMERS-CoV E/F junction at approximately nucleotide 24397 either uncut or cut with BglI. (*D*) Wild-type MERS-CoV, rMERS-CoV, and rMERS-CoV T1015N growth were compared in triplicate in Vero 81 cells (■, MERS-CoV; □, rMERS-CoV; ▲, rMERS-CoV T1015N). Error bars represent SD from the mean.

TRSs are thought to influence the abundance of upstream transcripts, it seems likely that the deletion of the regulatory domains of sgRNAs 3, 4, and 5 enhanced the expression of sgRNA2, resulting in increased S-glycoprotein expression and fusion phenotypes. An increased fusion phenotype was noted in rMERS-CoV-ΔORF3–5 that was rarely evident in wild-type or recombinant control virus-infected cells (Fig. 4 *C* and *D*).

Recombinant Virus Growth in Primary Lung Cultures. MERS-CoV has been reported to replicate in nonciliated HAEs and alveolar type II pneumocytes in ex vivo cultures (7, 13). To evaluate MERS-CoV tissue specificity in other lung cells, we obtained primary human lung fibroblasts, microvascular endothelial cells, alveolar type II pneumocytes, and ciliated HAEs and infected these cultures with MERS-CoV, rMERS-CoV-RFP, or rSARS-CoV. Wild-type MERS-CoV titers increased during infection in alveolar type II pneumocytes, microvascular endothelial cells, HAEs, and fibroblasts, approaching titers of 10^6 to 10^7 pfu/mL within 30 h postinfection (Fig. 5). RFP expression was clearly visible in fibroblast and ciliated HAE cultures but not in endothelial cells or alveolar type II pneumocytes, most likely due to high autofluorescence levels in these cultures (Fig. 6*A*). MERS-CoV replicated most efficiently in HAE and lung fibroblast cultures, slightly less efficiently in type II pneumocytes, and least efficiently in microvascular endothelial cells. Under identical conditions, SARS-CoV only replicated efficiently in the HAE cultures. To confirm robust MERS-CoV replication, we performed Northern blot analysis and clearly demonstrated the presence of both full-length and subgenomic-length MERS-CoV transcripts during virus infection of the primary lung cell types tested, with the exception of undifferentiated human bronchial cells (Fig. 6*B*). Consonant with these data, real-time RT-PCR and Western blot analysis demonstrated DPP4 mRNA and protein expression in all these cell types (Fig. 6 *C* and *D*).

Discussion

Rapid-response platforms are needed to control newly emerging virus pathogens. MERS-CoV likely emerged in the Middle East from exotic animals, perhaps bats, although the exact timing and origins of this pathogen in human populations remains unclear and is under study. MERS-CoV has caused 54 deaths at the time of writing (~50% mortality), including documented instances of human-to-human transmission (3, 8). Therefore, the epidemic potential of MERS-CoV is high and its biology, life cycle, gene function, and pathogenic mechanisms clearly warrant additional study.

Developing full-length infectious cDNAs of emerging RNA viruses is assisted by the availability of high-throughput sequencing, gene synthesis, and the use of class II/IIS restriction endonucleases that allow seamless assembly of consensus synthetic cDNA fragments into full-length infectious cDNAs. In this instance, we synthesized a molecular clone from the published sequence, assembled full-length genomes, and isolated recombinant viruses in culture. Recently, similar approaches have been applied to newly emerging influenza viruses and can direct the rapid assembly of genome-length microbial genomes exceeding millions of base pairs (10, 12, 14). It is noteworthy that rMERS-CoV replicated less efficiently than wild-type MERS-CoV, a phenotype that was linked to a tissue culture-adapted mutation in the S2 glycoprotein of the passage 9 stock of wild-type virus. S2 contains the fusion peptide, transmembrane domain, and two heptad repeat regions (HR1 and HR2), conserved features of class I fusion proteins that form the classic six-helix bundle believed to drive virion–cell membrane fusion (15). As substitutions in S2 may alter properties of S1 and S including stabilizing S1–S2 association, altering fusion behavior, and changing tissue tropism (16), it is likely that the T1015N mutation enhances entry and/or egress phenotypes in vitro. Although the origin of the tissue-culture adaptation is unclear, other studies have demonstrated the rapid emergence of tissue-culture adaptations in the M and S glycoproteins of human and zoonotic strains of SARS-CoV (17, 18). As our stock was derived from an inoculum used for primate experiments (19), it is possible that this tissue-culture adaptation altered MERS-CoV pathogenic outcomes after in vivo infection.

MERS-CoV, like other CoVs, expresses full-length and sgRNAs arranged in the form of a nested set from the 3′ end of the

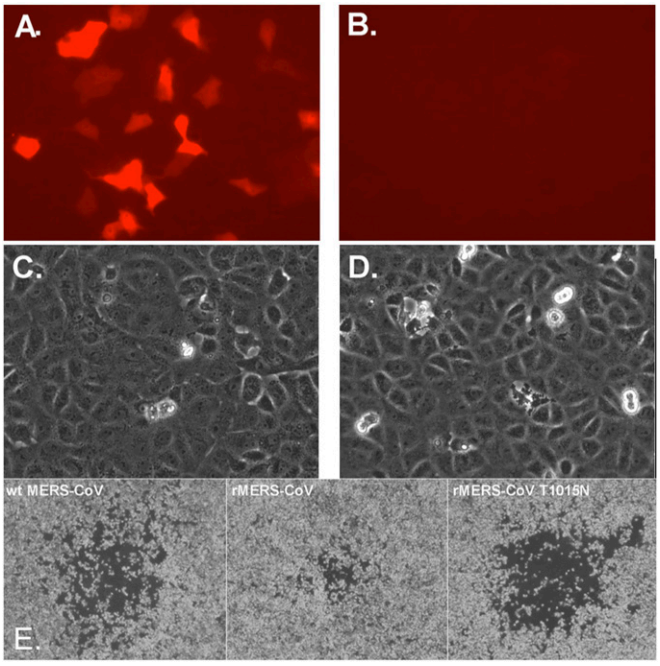

Fig. 3. rMERS-CoV-RFP expression and comparative plaque morphology. (*A–D*) Cultures of Vero cells were infected with rMERS-CoV-RFP (*A* and *C*) or rMERS-CoV (*B* and *D*). At 12 h postinfection, the cultures were visualized for tomato red fluorescence (*A* and *B*) or by light microscopy (*C* and *D*). (*E*) Plaque size differences between wild-type MERS-CoV, rMERS-CoV, and rMERS-CoV T1015N.

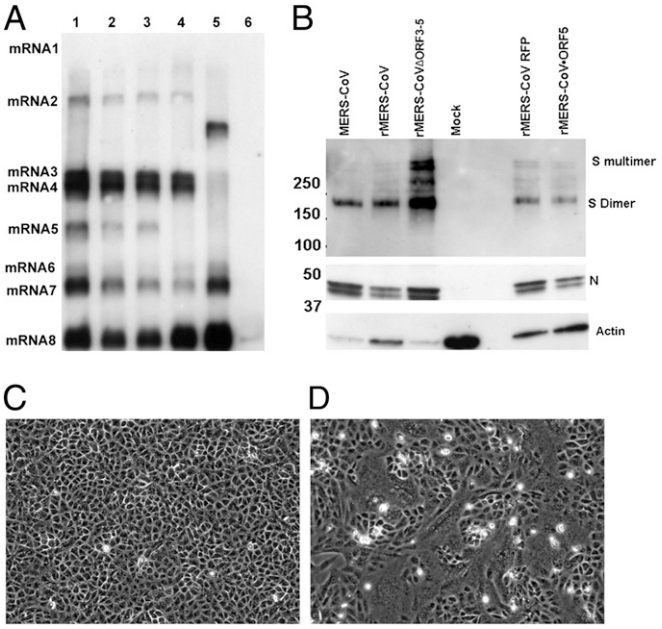

Fig. 4. Recombinant virus phenotypes. Cultures of cells were infected with MERS-CoV or recombinant derivative viruses, and intracellular RNA was harvested and analyzed by Northern blot (*A*; lane 1, MERS-CoV; lane 2, rMERS-CoV; lane 3, rMERS-CoV•ORF5; lane 4, rMERS-CoV-RFP; lane 5, rMERS-CoV-ΔORF3–5; lane 6, uninfected control). In parallel, cell lysates were resolved by SDS/PAGE and probed with anti-S and anti-N antibodies; increased S- but not N-protein expression levels were apparent in rMERS-CoV-ΔORF3–5–infected cells (*B*). *B* includes an actin control. rMERS-CoV-ΔORF3–5–infected cells (*D*) displayed an increased fusion phenotype compared with the parental control (*C*).

genome. The expression of sgRNAs is regulated by coordinated interactions between TRSs located at the 5′ end of the genome and just upstream of many downstream ORFs. Sequence analysis of a subset of the 5′ ends of sgRNAs encoding natural or indicator transgenes indicates that the core sequence AACGAA functions as a site for discontinuous transcription during negative-strand synthesis. MERS-CoV encodes several unique group-specific ORFs. Deletion analysis clearly demonstrates that these group-specific ORFs are not essential for virus replication, although the absence of these genes as a group attenuates peak viral titers (Fig. 2*A*). It is interesting that deletion of ORFs 3–5 resulted in enhanced expression of sgRNA2, which encodes the S glycoprotein. These findings are consistent with a model of discontinuous transcription during negative-strand synthesis, where downstream TRSs influence the abundance of upstream transcripts (20). Increased sgRNA2 transcript production resulted in enhanced S-glycoprotein expression that was associated with increased syncytial formation following MERS-CoV-ΔORF3–5 infection (Fig. 4*D*). Increased syncytia formation and in vitro cytotoxicity may translate to improved cell-to-cell spread and/or altered in vivo pathogenesis, but this phenotype is complicated by the loss of several group-specific ORFs. Wild-type and recombinant S glycoprotein is heavily glycosylated in vitro, as PNGase F removes *N*-linked glycosylation moieties and reduces S-glycoprotein molecular weights by ∼50 kDa. According to the NetOGlyc 4.0 Server (www.cbs.dtu.dk/services/NetOGlyc), the MERS-CoV S glycoprotein is also predicted to encode three *O*-linked glycosylation sites, so PNGase F treatment will likely not remove all carbohydrate moieties.

Currently, the functions of the MERS-CoV group-specific ORFs are unknown, but by analogy with other CoVs, they likely encode structural proteins or IFN antagonist genes that modulate in vivo replication efficiency and/or pathogenesis (21). Unfortunately, we have not been able to demonstrate MERS-CoV replication in standard laboratory strains of *Mus mus musculus, M. m. domesticus*, or *M. m. castaneus* mice, nor have we been able to establish infections in immune-deficient mice, perhaps due to problems in receptor binding and entry (7). In support of this hypothesis, sequence and structural comparisons of the SARS-CoV S-glycoprotein receptor-binding domain bound with human DPP4 receptor reveal differences between several key interface residues in mouse DPP4 compared with human DPP4 that likely disrupt binding (22). The development of a macaque model (19), coupled with a robust genetic system for MERS-CoV, provides a platform for evaluating the underlying roles of MERS-CoV genes in viral pathogenesis in vivo.

SARS-CoV primarily targeted ciliated HAEs and type 1 and 2 pneumocytes in the lung (13, 23). In ex vivo human lung cultures, MERS-CoV is reported to infect and replicate in nonciliated bronchial epithelium, bronchiolar epithelial cells, alveolar epithelial cells, and perhaps endothelial cells (13). Previously, we demonstrated that HAEs provide a robust primary cell substrate for culturing uncultivable viruses such as human CoVs (11). We extend these studies by demonstrating DPP4 transcript, protein expression, and MERS-CoV replication in purified primary alveolar type II pneumocytes and microvascular endothelial and fibroblast cultures. Under identical conditions, SARS-CoV did not replicate efficiently in microvascular endothelial and fibroblast cultures, likely reflecting the unique tissue expression patterns of

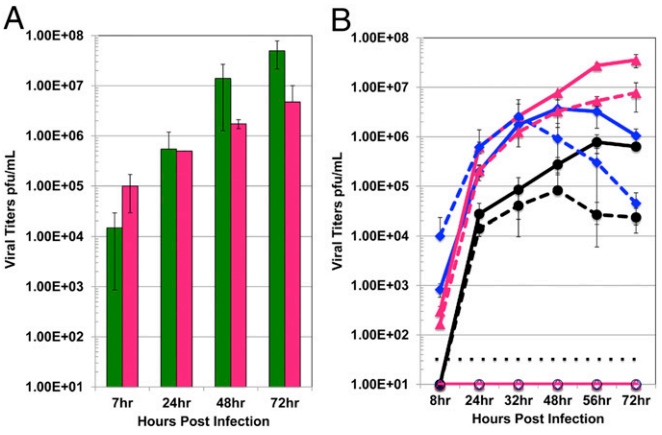

Fig. 5. Recombinant virus growth in primary human lung cells. HAEs, primary alveolar type II pneumocytes, primary lung microvascular endothelial cells, and primary lung fibroblast cells were infected with wild-type rSARS-CoV, wild-type MERS-CoV, or rMERS-CoV-RFP. (*A*) Wild-type MERS-CoV and SARS-CoV growth kinetics in HAEs. Data are representative of two independent experiments. Error bars represent SD from the mean. Green bars, wild-type SARS-CoV; pink bars, wild-type MERS-CoV. (*B*) Wild-type SARS-CoV, wild-type MERS-CoV, and rMERS-CoV-RFP growth kinetics were compared in alveolar type II (ATII) pneumocytes, lung microvascular endothelial (MVE) cells, and lung fibroblasts (FBs). SARS-CoV did not replicate in any of the primary cell types examined in *B*. Cells were specific to one of two donors, and neither was permissive for SARS-CoV. Data are representative of two independent experiments. Error bars represent SD from the mean. The dotted black line in *B* represents the limit of detection for the assay. All points under this line are considered to be negative for replication in the samples assayed. Solid blue line with closed diamond, wild-type MERS-CoV in ATII cells; dotted blue line with closed diamond, rMERS-CoV-RFP in ATII cells; solid blue line with open diamond, wild-type SARS-CoV in ATII cells (did not replicate); solid pink line with closed triangle, wild-type MERS-CoV in FB cells; dotted pink line with closed triangle, rMERS-CoV-RFP in FB cells; solid pink line with open triangle, wild-type SARS-CoV in FB cells (did not replicate); solid black line with closed circle, wild-type MERS-CoV in MVE cells; dotted black line with closed circle, rMERS-CoV-RFP in MVE cells; solid black line with open circle, wild-type SARS-CoV in MVE cells (did not replicate).

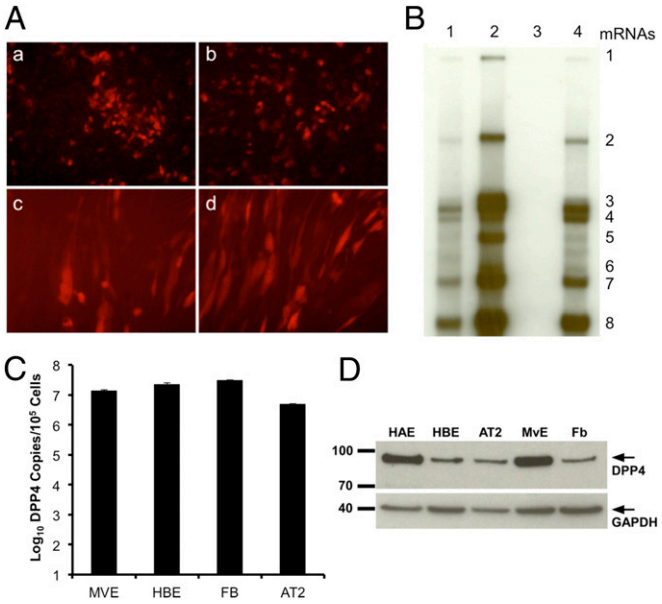

Fig. 6. Recombinant virus expression in primary human lung cells. (*A* and *B*) HAE and FB cultures were infected with rMERS-CoV-RFP and visualized by fluorescent microscopy [20×; (*A*, *a*) HAE, 48 h; (*A*, *b*) HAE, 72 h; (*A*, *c*) FB, 48 h; (*A*, *d*) FB, 72 h]. MERS-CoV intracellular RNA was harvested and analyzed by Northern blot (*B*; lane 1, primary alveolar type II pneumocytes; lane 2, primary lung fibroblasts; lane 3, primary undifferentiated airway epithelium; lane 4, primary lung microvascular endothelial cells). Images are representative of two independent experiments. (*C* and *D*) Real-time RT-PCR and Western blot analysis of DPP4 expression in primary human cells. AT2, alveolar type II pneumocytes; HAE, human airway epithelial cells under an air–liquid interface.

the angiotensin-converting enzyme 2 and DPP4 receptors. Using this patient code, we did not observe SARS-CoV replication in alveolar type II pneumocytes, nor did we detect robust MERS-CoV replication in nondifferentiated human bronchial epithelial (HBE) cells. As previously noted (24), genetic susceptibility allele patterns in different patient codes might influence virus infection outcomes and replication efficiency. The data likely underscore the importance of correlating CoV infectivity patterns with DPP4 and TMPRSS2 expression in human tissues (25). Although speculative, the demonstration of efficient MERS-CoV replication in endothelial cells may provide a pathway for spread from the lung to other organs. Interestingly, highly pathogenic H5N1 strains also replicate efficiently in microvascular endothelial cells, potentially providing a pathway for systemic spread to other organs (26, 27).

The availability of a MERS-CoV molecular clone and recombinant viruses expressing indicator genes such as RFP provides important tools for high-throughput screening of candidate antiviral agents such as IFN, kinase inhibitors, and inhibitors of viral cellular proteases that are essential for polyprotein processing or virus docking and entry into cells. The molecular clone will assist in the identification and validation of genes targeted by antivirals and in the discovery of virally encoded functions important for virus replication and pathogenesis. Finally, the molecular clone may provide the capacity to rationally design live-attenuated virus vaccines (28) or safer seed stocks for killed vaccines that lack genes or genetic functions that are critical for regulating in vivo pathogenesis for other alpha- and betacoronaviruses.

Materials and Methods

Virus and Cells. The wild-type EMC2012 strain of MERS-CoV (passage 8, designated MERS-CoV) was provided by Bart Haagmans (Erasmus University, Rotterdam). Virus stocks (passage 9) were propagated on Vero 81 cells (CCL-81; ATCC) in reduced-serum minimal essential medium (Opti-MEM) containing 4% (vol/vol) fetal clone II serum (HyClone/Gibco) and supplemented with kanamycin (0.25 μg/mL) and gentamycin (0.05 g/mL) at 37 °C in a humidified CO_2 incubator. For wild-type and recombinant virus growth, cultures of Vero cells were infected at a multiplicity of infection (MOI) of 0.01 or 1.0 as indicated for 1 h, and samples were titered by plaque assay. Recombinant SARS-CoV strain Urbani was propagated on Vero E6 cells in MEM containing 10% fetal clone II serum and supplemented with kanamycin and gentamycin. Virus plaques were visualized by neutral red staining at 2–3 d postinfection. Virus was maintained under biosafety level (BSL)3 conditions with redundant fans, and personnel used powered-air purifying respirators and Tyvek suits.

Human lungs were obtained under protocol 03-1396, which was approved by the University of North Carolina at Chapel Hill Biomedical Institutional Review Board, and donors gave informed consent. Tracheo-bronchial and alveolar epithelial cells were obtained and cultured (29, 30). Human lung microvascular endothelial cells were obtained by dispase and elastase digestion of peripheral lung tissue stripped of the visceral pleura, followed by primary culture in EGM-2 media plus FBS (Lonza). The cells were subjected to two or three rounds of CD31 bead purification (Dynabeads; Life Technologies/Invitrogen), after which they were >95% CD31-positive as measured by flow cytometry and used between passages 5 and 10. Primary human lung fibroblasts were obtained by outgrowth from finely minced distal human lung tissues onto scratched type 1/3 collagen-coated dishes in Dulbecco's modified Eagle medium with high glucose (DMEMH) media plus 10% FBS, antibiotics, and antimycotics. Primary isolated cells were obtained by treatment with trypsin/EDTA and subcultured as above. The cells exhibited typical fibroblast morphology and were negative for CD31 and pan-cytokeratin as assessed by flow cytometry and immunofluorescence staining. To evaluate dipeptidyl peptidase 4 expression from primary lung cultures, RNA was reverse-transcribed (SuperScript III; Invitrogen) and then subjected to quantitative RT-PCR analysis for DPP4 copy-number determination (iQ SYBR Green Supermix; Bio-Rad). Primers were as follows: DPP4F (5′-ccaaagactgtacgggttcc-3′) and DPP4R (5′-acaaagaactttacagttggattcac-3′); and GAPDHF (5′-agccacatcgctcagacac-3′) and GAPDHR (5′-gcccaatacgaccaaatcc-3). Raw DPP4 results were normalized to GAPDH and fit to a standard curve made using plasmids encoding DPP4.

Systematic Assembly of a Full-Length MERS-CoV cDNA. The clone was designed and purchased from Bio Basic as six contiguous cDNAs flanked by unique class II restriction endonuclease sites (BglI). We used published sequence information from an earlier reported passage (9). The MERS D fragment was unstable and subsequently subdivided into two subclones designated MERS D1 and D2 containing mutations $G_{494}C$ and $G_{17713}T$ to disrupt two naturally occurring BglI sites and an $A_{2849}G$ mutation to disrupt a stretch of eight A residues, which might interfere with in vitro RNA transcription reactions. In addition, several silent mutations were included to produce unique BglI sites at appropriate locations across the genome (Fig. 1). The MERS A–F inserts were restriction-digested, resolved on 0.8% agarose gels, and visualized, excised, and purified using a QIAquick Gel Extraction Kit (Qiagen). The MERS A–F inserts were mixed and ligated overnight at 4 °C, phenol/chloroform-extracted, and precipitated with isopropyl alcohol. Full-length T7 transcripts were generated in vitro as described by the manufacturer (Ambion; mMessage mMachine) with certain modifications (12). For MERS-CoV N transcripts, 1 μg of plasmid DNA encoding the N gene (amplified using forward primer 5′-atttaggtgacactatagatggcatcccctgctgcacc-3′ and reverse primer 5′-ttttttttttttttttttttttttctaatcagtgttaacatcaatcattgg-3′) was transcribed by SP6 RNA polymerase with a 4:1 ratio of cap analog to GTP.

Recombinant MERS-CoV Deletion and Expression Constructs. The reported sequence of MERS-CoV strain EMC2012 identified a mutation at position $G_{27162}A$, which resulted in a stop codon at position 108 in ORF5 and which had been incorporated into the synthetic clone, resulting in the rMERS-CoV•ORF5 recombinant. To restore ORF5, the MERS F plasmid was PCR-amplified with either primer set EMC F+1865 (5′-tccaaccaacacactatgtc-3′) and EMC F-2820 (5′-nnnnnngctcttcaaagtattatgaggataactaag-3′) or set EMC F+2830 (5′-nnnnnngctcttcactttggtttgtagatagaattcg-3′) and EMC F-3941 (5′-caccgaaatgcatgccagcc-3′). To make rMERS-CoV wild-type virus, the two PCR amplicons were digested with SapI, ligated together, digested with PflMI, and then cloned into PflMI-digested F plasmid. Sequence analysis of MERS-CoV EMC2012 p9 material also revealed a consensus T1015N mutation in the S glycoprotein that was not present in the cDNA clone. We used standard recombinant DNA approaches to produce the rMERS-CoV T1015N virus.

To replace ORF5 with the RFP gene, one amplicon was generated by amplifying the F plasmid with primers EMC F+1376 (5′-gtttctgtcgatcttgagtc-3′) and F2463Rev (5′-nnnnnncgtctcaccatagttcgttaaaatcctgg-3′). A second PCR

MICROBIOLOGY

amplified the RFP gene with primers tRFPbsmb (5′-nnnnnncgtctctatggtgagcaagggcgagg-3′) and tRFP rev (5′-nnnnnngggacccttacttgtacagctcgtccatg-3′). The two amplicons were digested with BsmBI and then joined with T4 DNA ligase. The product was digested with PacI and SanDI and ligated into the MERS F plasmid using standard techniques. To delete ORFs 3–5, the MERS F plasmid was amplified with primer M13F1 and primer EMC F-1140 (5′-nnnnnngggaccctaattagtgaacatgaaccttatg-3′). This product was digested with NruI and SanDI and ligated into the MERS F plasmid.

Transfection of Full-Length Transcripts. RNA transcripts were added to 800 μL of Vero cell suspension (8.0×10^6 cells) in an electroporation cuvette, and four electrical pulses of 450 V at 50 μF were delivered with a Gene Pulser II electroporator (Bio-Rad). The transfected Vero cells were allowed to recover for 10 min at room temperature and then incubated at 37 °C for 2–4 d in a 75-cm^2 flask. Virus progeny was then passaged one time in Vero cells for 48 h and used to generate a stock for future use.

Restriction Fragment Length Polymorphism Analysis. To detect leader-containing RNAs, intracellular RNA from wild-type, rMERS-CoV, and derivative viruses was reverse-transcribed with a primer at the 3′ end of the genome and cDNA was isolated for PCR using a reverse primer located in ORF5 and a forward primer located in the leader RNA sequence at the 5′ end of the genome (5′-ctatctcacttcccctcgttctc-3′). Leader-containing amplicons were sequenced (14). For RT-PCR restriction length polymorphism analysis, primers EMC 36F (5′-ccgatattctggtggttgat-3′) (nucleotides 17310–17329 genome) and EMC 37R (5′-atcgagtttaaagcccatcc-3′) (nucleotides 18171–18190 genome) were used to amplify an ∼880-bp–long amplicon spanning a naturally occurring BglI site at nucleotide 17717 (9). In addition, primers EMC 50F (5′-ccaatttacgccaggatgat-3′) (nucleotides 23968–23987) and EMC 51R (5′-attaagggaggtaatgggct-3′) (nucleotides 25039–25058) amplified an ∼1,090-bp region that spans the E/F junction in recombinant MERS-CoV (nucleotide 24397). Wild-type MERS-CoV cDNA product cannot be cleaved with BglI in this region, whereas the recombinant virus PCR amplicon contains an engineered BglI site between nucleotides 24391 and 24401.

Northern and Western Blot Analysis. At 12 h postinfection, intracellular RNA was isolated using TRIzol reagent (Invitrogen). RNA (∼0.1 μg) was treated with glyoxal and separated on agarose gels using NorthernMax-Gly according to the manufacturer's directions (Ambion). The RNA was transferred to a BrightStar-Plus membrane (Ambion) for 3–4 h and then cross-linked to the membrane using UV light. The blot was prehybridized and probed with a MERS-CoV N gene-specific biotinylated oligodeoxynucleotide probe. After washing, filters were incubated with streptavidin-alkaline phosphatase, washed, and then incubated with the chemiluminescent substrate CDP-Star (Sigma). The blots were overlaid with film and developed.

For Western blot analyses, 12 h postinfection, wild-type MERS-CoV–, rMERS-CoV–, rMERS-CoV-RFP–, rMERS-CoV•ORF5–, and rMERS-CoV-ΔORF3–5–infected cells were washed in 1× PBS and lysed in buffer containing 20 mM Tris·HCl (pH 7.6), 150 mM NaCl, 0.5% deoxycholine, 1% Nonidet P-40, and 0.1% SDS. Postnuclear supernatants were then added to an equal volume of 5 mM EDTA, 0.9% SDS, resulting in a final SDS concentration of 0.5%. Samples were then heat-inactivated for 30 min at 90 °C at BSL3 before removal. At BSL2, samples were again heat-inactivated for 30 min at 90 °C before use. Equivalent sample volumes were loaded onto 7.5% Criterion gradient gels (Bio-Rad) and transferred to PVDF membranes (Bio-Rad). For detecting MERS-CoV antigens, blots were probed with polyclonal mouse antisera obtained after vaccination of mice with Venezuelan equine encephalitis virus replicon particles that express the MERS-CoV S glycoprotein (VRP-S) or N protein (VRP-N) (each diluted 1:400) and developed using ECL chemiluminescence reagents (Amersham Biosciences). Antiserum against mouse actin proteins was used as a control. For detection of DPP4 protein, a DPP4 antibody (LifeSpan BioSciences) or GAPDH mouse monoclonal antibody was used for Western blot analysis (1:10,000; Sigma).

ACKNOWLEDGMENTS. We thank the University of North Carolina (UNC) Lineberger Comprehensive Cancer Center DNA Sequencing Facility, the Nucleic Acids Division of the Lineberger Tissue Culture Facility, the UNC Cystic Fibrosis Tissue Procurement and Cell Culture Core for providing primary human cells, the UNC Nucleic Acid Core, and the UNC Genome Analysis Facility. This work was supported by grants from the National Institutes of Health (U19AI100625, U19AI107810, AI108197, and AI085524) and Defense Threat Reduction Agency (DTRA) HDTRA1-12-C-0035.

1. Tsushima K, et al. (2009) Acute lung injury review. *Intern Med* 48(9):621–630.
2. Baric RS, Yount B, Hensley L, Peel SA, Chen W (1997) Episodic evolution mediates interspecies transfer of a murine coronavirus. *J Virol* 71(3):1946–1955.
3. Zaki AM, van Boheemen S, Bestebroer TM, Osterhaus AD, Fouchier RA (2012) Isolation of a novel coronavirus from a man with pneumonia in Saudi Arabia. *N Engl J Med* 367(19):1814–1820.
4. Huynh J, et al. (2012) Evidence supporting a zoonotic origin of human coronavirus strain NL63. *J Virol* 86(23):12816–12825.
5. Perlman S, Netland J (2009) Coronaviruses post-SARS: Update on replication and pathogenesis. *Nat Rev Microbiol* 7(6):439–450.
6. Gierer S, et al. (2013) The spike protein of the emerging betacoronavirus EMC uses a novel coronavirus receptor for entry, can be activated by TMPRSS2, and is targeted by neutralizing antibodies. *J Virol* 87(10):5502–5511.
7. Raj VS, et al. (2013) Dipeptidyl peptidase 4 is a functional receptor for the emerging human coronavirus-EMC. *Nature* 495(7440):251–254.
8. Memish ZA, Zumla AI, Al-Hakeem RF, Al-Rabeeah AA, Stephens GM (2013) Family cluster of Middle East respiratory syndrome coronavirus infections. *N Engl J Med* 368(26):2487–2494.
9. van Boheemen S, et al. (2012) Genomic characterization of a newly discovered coronavirus associated with acute respiratory distress syndrome in humans. *MBio* 3(6): e00473-12.
10. Becker MM, et al. (2008) Synthetic recombinant bat SARS-like coronavirus is infectious in cultured cells and in mice. *Proc Natl Acad Sci USA* 105(50):19944–19949.
11. Donaldson EF, et al. (2008) Systematic assembly of a full-length infectious clone of human coronavirus NL63. *J Virol* 82(23):11948–11957.
12. Yount B, et al. (2003) Reverse genetics with a full-length infectious cDNA of severe acute respiratory syndrome coronavirus. *Proc Natl Acad Sci USA* 100(22):12995–13000.
13. Chan RW, et al. (2013) Tropism of and innate immune responses to the novel human betacoronavirus lineage C virus in human ex vivo respiratory organ cultures. *J Virol* 87(12):6604–6614.
14. Yount B, Roberts RS, Lindesmith L, Baric RS (2006) Rewiring the severe acute respiratory syndrome coronavirus (SARS-CoV) transcription circuit: Engineering a recombination-resistant genome. *Proc Natl Acad Sci USA* 103(33):12546–12551.
15. Bosch BJ, et al. (2004) Severe acute respiratory syndrome coronavirus (SARS-CoV) infection inhibition using spike protein heptad repeat-derived peptides. *Proc Natl Acad Sci USA* 101(22):8455–8460.
16. McRoy WC, Baric RS (2008) Amino acid substitutions in the S2 subunit of mouse hepatitis virus variant V51 encode determinants of host range expansion. *J Virol* 82(3):1414–1424.
17. Rockx B, et al. (2007) Synthetic reconstruction of zoonotic and early human severe acute respiratory syndrome coronavirus isolates that produce fatal disease in aged mice. *J Virol* 81(14):7410–7423.
18. Pacciarini F, et al. (2008) Persistent replication of severe acute respiratory syndrome coronavirus in human tubular kidney cells selects for adaptive mutations in the membrane protein. *J Virol* 82(11):5137–5144.
19. Munster VJ, de Wit E, Feldmann H (2013) Pneumonia from human coronavirus in a macaque model. *N Engl J Med* 368(16):1560–1562.
20. Sawicki SG, Sawicki DL (2005) Coronavirus transcription: A perspective. *Curr Top Microbiol Immunol* 287:31–55.
21. Totura AL, Baric RS (2012) SARS coronavirus pathogenesis: Host innate immune responses and viral antagonism of interferon. *Curr Opin Virol* 2(3):264–275.
22. Wang N, et al. (2013) Structure of MERS-CoV spike receptor-binding domain complexed with human receptor DPP4. *Cell Res* 23(8):986–993.
23. Dijkman R, et al. (2013) Isolation and characterization of current human coronavirus strains in primary human epithelial cell cultures reveal differences in target cell tropism. *J Virol* 87(11):6081–6090.
24. Sims AC, et al. (2013) Release of severe acute respiratory syndrome coronavirus nuclear import block enhances host transcription in human lung cells. *J Virol* 87(7): 3885–3902.
25. Leow MK (August 13, 2013) Correlating cell line studies with tissue distribution of DPP4/TMPRSS2 and human biological samples may better define the viral tropism of MERS-CoV. *J Infect Dis*, 10.1093/infdis/jit330.
26. Zeng H, et al. (2012) Human pulmonary microvascular endothelial cells support productive replication of highly pathogenic avian influenza viruses: Possible involvement in the pathogenesis of human H5N1 virus infection. *J Virol* 86(2):667–678.
27. Chan MC, et al. (2009) Influenza H5N1 virus infection of polarized human alveolar epithelial cells and lung microvascular endothelial cells. *Respir Res* 10:102.
28. Graham RL, et al. (2012) A live, impaired-fidelity coronavirus vaccine protects in an aged, immunocompromised mouse model of lethal disease. *Nat Med* 18(12): 1820–1826.
29. Fulcher ML, Randell SH (2013) Human nasal and tracheo-bronchial respiratory epithelial cell culture. *Methods Mol Biol* 945:109–121.
30. Bove PF, et al. (2010) Human alveolar type II cells secrete and absorb liquid in response to local nucleotide signaling. *J Biol Chem* 285(45):34939–34949.